minerals

MDPI

Review

Mineralogy, Crystallography and Structural Complexity of Natural Uranyl Silicates

Jakub Plášil

Institute of Physics ASCR, v.v.i., Na Slovance 1999/2, 18221 Prague 8, Czech Republic; plasil@fzu.cz; Tel.: +420-775-21-27-57

Received: 10 October 2018; Accepted: 19 November 2018; Published: 27 November 2018

Abstract: Naturally occurring uranyl silicates are common constituents of the oxidized parts (i.e., supergene zone) of various types of uranium deposits. Their abundance reflects the widespread distribution of Si^{4+} in the Earth's crust and, therefore, in groundwaters. Up to date, 16 uranyl silicate minerals are known. Noteworthy is that the natural uranyl silicates are not extremely diverse regarding their crystal structures; it is a result of possible concentrations (activity) of Si^{4+} in aqueous solutions derived from dissolution of primary Si minerals or the composition of late hydrothermal fluids. Therefore, in natural systems, we distinguish in fact among two groups of uranyl silicate minerals: uranophane and weeksite-group. They differ in U:Si ratio (uranophane, 1:1; weeksite, 2:5) and they form under different conditions, reflected in distinctive mineral associations. An overview of crystal-chemistry is provided in this paper, along with the new structure data for few members of the uranophane group. Calculations of the structural complexity parameters for natural uranyl silicates are commented about as well as other groups of uranyl minerals; these calculations are also presented from the point of view of the mineral paragenesis and associations.

Keywords: uranyl silicate; crystal structure; structural hierarchy; chemical composition; complexity measures; evolution

1. Introduction

Uranyl silicates minerals are typical representatives of the oxidized parts of uranium deposits worldwide [1–5], forming during oxidizing weathering of uraninite, ideally UO_2, or coffinite, ideally $U(SiO_4)$. The abundance of occurrences reflects the widespread distribution of Si^{4+} in the Earth's crust [5]. Besides the important role that uranyl silicate minerals play in the evolution of U deposits and controlling the mobility of U in their oxide-zones [6], they were also identified as alteration products of spent nuclear fuel, which may have a significant impact upon the mobility of U and other radionuclides under geological repository conditions [7–10].

To date, the group of naturally occurring uranyl silicates comprises 16 mineral members (Table 1). However, some of them remain only poorly defined. The crystal-chemistry of uranyl silicates attracted much attention for a long time [11–20] namely in connection with the increased attention due to spent nuclear fuel waste management. Infrared and Raman spectroscopy data for natural uranyl silicates have been reported by [21] and also recently by a thorough review of Raman spectroscopy of uranyl minerals and phases [22]. With increased attention many synthetic uranyl silicate compounds have been synthesized, usually with crystal chemistry divergent from the natural ones [23–29], and also both experimental [30–32] and theoretical studies [33,34] have been undertaken in order to determine the thermodynamic properties of uranyl silicate minerals.

A review of uranyl silicates mineralogy has been most recently done years ago by [14]. This paper aims to provide an overview of the known naturally occurring uranyl silicates, their mineralogy and crystal chemistry (including new crystal-structure data) and their complexity (information

measures) with some implications for their occurrence. Moreover, it provides new diffraction data for sklodowskite, cuprosklodowskite, oursinite, and soddyite, including refinements of the H atoms, which remained undetermined for some of them until now. It also aims to overcome a few inconsistencies regarding the structures and mineralogy of natural uranyl silicates that still appear in the literature.

Table 1. Uranyl silicate minerals.

Mineral	Chemical Composition	Unit Cell (a, b, c, (Å), α, β, γ (°)); Space Group	References
Uranophane group			
Boltwoodite	$K[(UO_2)(SiO_3OH)](H_2O)_{1.5}$	7.077, 7.060, 6.648, 90, 104.98, 90; $P2_1/m$	[35]
Natroboltwoodite	$Na[(UO_2)(SiO_3OH)](H_2O)_{1.5}$?		[35]
Cuprosklodowskite	$Cu[(UO_2)(SiO_3OH)]_2(H_2O)_6$	6.655, 7.057, 9.234, 70.43, 70.95, 89.85; $P\bar{1}$	[11], this work
Kasolite	$Pb[(UO_2)(SiO_4](H_2O)$	6.705, 6.926, 13.286, 90, 105.06, 90; $P2_1/c$	[13,19]
Oursinite	$(Co_{0.8}Mg_{0.2})[(UO_2)(SiO_3OH)]_2(H_2O)_6$	7.046, 17.545, 12.723, 90, 90, 90; *Cmce*	[17], this work
Sklodowskite	$Mg[(UO_2)(SiO_3OH)]_2(H_2O)_6$	17.408, 7.043, 6.608, 90, 105.88, 90; $C2/m$	[12], this work
Uranophane-α	$Ca[(UO_2)(SiO_3OH)]_2(H_2O)_5$	15.909, 7.002, 6.665, 90, 97.27, 90; $P2_1$	[16]
Uranophane-β	$Ca[(UO_2)(SiO_3OH)]_2(H_2O)_5$	6.626, 15.455, 13.951, 90, 91.44, 90, $P2_1/c$	[36]
Swamboite-(Nd)	$Nd_{0.333}[(UO_2)(SiO_3OH)](H_2O)_{2.41}$	6.656, 6.988, 8.806, 90, 102.59, 90; *	[37]
Weeksite group			
Weeksite	$K_2(UO_2)_2(Si_5O_{13})(H_2O)_4$	14.196, 14.229, 9.631, 90, 111.58, 90; $C2/m$	[18]
Haiweeite	$Ca[(UO_2)_2(SiO_3OH)_2(Si_3O_6)](H_2O)_6$	18.300, 14.233, 17.919, 90, 90, 90; *Pbcn*	[19]
Coutinhoite	$Th_xBa_{1-2x}(H_2O)_y[(UO_2)_2(Si_5O_{13})](H_2O)_3$	14.168, 14.194, 35.754, 90, 90, 90; *Cmmb*	[38]
Soddyite	$(UO_2)_2(SiO_4)(H_2O)_2$	8.310, 11.221, 18.658, 90, 90, 90; *Fddd*	[39], this work
Poorly defined			
Calcioursilite	$Ca_4(UO_2)_4(Si_2O_5)_5(OH)_6(H_2O)_{15}$		[40–42]
Magnioursilite	$Mg_4(UO_2)_4(Si_2O_5)_5(OH)_6(H_2O)_{20}$		[40–42]
Uranosilite	$UO_3{\cdot}7SiO_2$?		[43]

*—structure is (3 + 3)-commensuratelly modulated, of the super-space group $P2_1/m(a1, b1, g1)00(-a1, b1, g1)00(a2, 0, g2)0s$ with a modulation-vector (1/3, 1/3, 0), (−1/3, 1/3, 0), (1/2, 0, 1/2). ?—chemical composition is highly questionable.

2. Experiment

2.1. Single-Crystal X-Ray Diffraction

New single-crystal X-ray data were collected for sklodowskite, cuprosklodowskite, oursinite, and soddyite. Crystals used in the study were retrieved from the collections of the National Museum in Prague (cuprosklodowskite) and Museum of Natural History in Luxembourg (sklodowskite, oursinite, and soddyite).

Intensity data were collected using two different X-ray diffractometers (XRD). (1) Rigaku SuperNova single-crystal diffractometer connected with the Atlas S2 CCD detector; equipped with Mo micro-focus X-ray tube, working at 50 kV and 0.8 mA (40 W), providing a beam spot of ~120 μm; and (2) Oxford Diffraction Gemini single-crystal diffractometer equipped with the Atlas CCD detector and using monochromated Mo$K\alpha$ radiation from a sealed X-ray tube, operating at 50 kV and 35 mA (1500 W), collimated with a fiber-optics Mo-Enhance collimator. Data processing was done using CrysAlis pro software [44].

For the structure solution, SHELXT software [45] was used and structures were subsequently refined by Jana2006 [46] against F^2. Hydrogen atom positions were localized from the difference Fourier maps and the H atoms found were treated by the mixture of independent and constrained refinement. The resulting R values are given in overview in Table 2. Crystallographic information files were deposited as Supplementary files.

Table 2. Crystallographic data for uranyl silicate minerals studied by single-crystal X-ray diffraction (XRD).

Mineral	*a*, *b*, *c* (Å)	α, β, γ (°)	R_1 (%)	No. ($I > 3\sigma$ (I))
Sklodowskite	17.4078(6), 7.0428(3), 6.6080(2)	90, 105.882(14), 90	1.96	836
Cuprosklodowskite	6.6549(5), 7.0573(4), 9.2344(8)	70.429(6), 70.945(7), 89.850(5)	3.75	1033
Oursinite	7.0457(4), 17.5445(8), 12.7231(2)	90, 90, 90	2.03	976
Soddyite	8.3097(3), 11.2205(4), 18.6576(11)	90, 90, 90	1.92	499

2.2. Complexity Calculations and a Bond-Valence Approach

The structural complexity, the Shannon information content per atom (I_G) and per unit cell ($I_{G,total}$), were calculated using an approach proposed in [47,48], as follows: the complexity of a crystal structure can be characterized quantitatively by the amount of Shannon information, which is measured in bits (binary digits) per atom (bits/atom) and per unit cell (bits/cell), respectively. The concept used herein of Shannon information, also known as Shannon entropy, originates from information theory. The amount of Shannon information reflects the diversity and relative proportion of different objects e.g., the number and relative proportion of different sites in an elementary unit cell of a crystal structure. The corresponding equations can be found in the references given above. The information based structural-complexity parameters for hereby studied uranyl silicates were calculated using the crystal-structure data by the software package TOPOS [49]. The surrogate H atoms were used in calculations to calculate also the contribution of the H atoms to the overall complexity of the minerals, where structure data lack information about H atoms.

The chemical complexity was estimated by considering chemical formula as a message, where symbols correspond to different chemical elements, and it was calculated equivalently to the structural complexity following the approach given by [50].

3. Mineralogy and Crystallography of Natural Uranyl Silicates

Based on the U:Si ratio, uranyl silicates may be subdivided into three major groups: the uranophane group (1:1), weeksite and haiweeite (2:5), and soddyite (2:1). The vast majority of natural uranyl silicate structures are based upon sheets topologies, with a few minerals containing heteropolyhedral frameworks. The higher the U:Si ratio (i.e., the higher Si concentration) the higher is the degree of polymerization of silicate tetrahedra. An increase of the U:Si ratio is also related to a change of linkage mode between U and Si polyhedra, from edge- to corner-sharing. The high U:Si is characteristic for the synthetic compounds [23–29], which will not be mentioned in the following text. The approach concerning secondary-building units (SBUs)is a useful tool for highlighting differences in mineral groups mentioned above. This approach has been recently successfully applied to a group of synthetic uranyl silicates and germanates, mostly having framework structures [29]. In the case of natural uranyl silicates the two SBUs can be identified, both of them with five-connected U atoms (Figure 1). The first type, with U_2Si_2 tetramers, is typical for the uranophane group of minerals, while the second type, where three additional Si tetrahedra are linked to U_2Si_2 to form U_2Si_5 heptamers, is characteristic of the weeksite group of minerals.

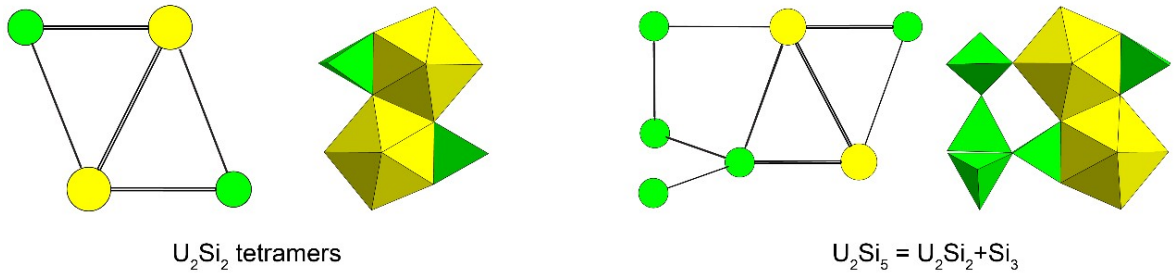

Figure 1. Connectivity in secondary-building-units (SBUs) in natural uranyl silicates shown in ball-and-stick and polyhedral representation (U = yellow, Si = green).

3.1. Uranophane Group (1:1)

The best-known representatives of the group, and also the most frequently occurring, are **uranophane-α** (commonly called uranophane) (Figure 2a) and **uranophane-β** (Figure 2b). They are both monoclinic polymorphs of $Ca[(UO_2)_2(SiO_3OH)_2]\cdot 5H_2O$. While uranophane-α crystallizes in the space group $P2_1$, the structure of uranophane-β adopts $P2_1/c$. All minerals of this group are based upon layered structures, with sheets of so-called uranophane topology (Figure 3a) that contain

(UO_7) pentagonal bipyramids and acid [SiO_3(OH)] groups (except of kasolite, which contains SiO_4 groups), occupying triangles of the topology. The pentagonal bipyramids form edge-sharing chains that are connected by Si-tetrahedra. In minerals with the uranophane type of sheets there are several orientational isomers, differing in the orientation of the free vertices of the SiO_4 tetrahedra pointing up (***u***) or down (***d***) relative to the plane of the sheets [17]. For example, both uranophane-α and uranophane-β have PT (pentagon-triangles) chains with vertices of tetrahedra pointing all ***up*** or all ***down*** (Figure 3b,c), while for an ST (square-triangles) chain there is a . . . ***ududud*** . . . the sequence for uranophane-α (Figure 3b) and . . . ***uudduudd*** . . . sequence for uranophane- β (Figure 3c) [36]. Adjacent sheets of U-Si polyhedra are linked through the O_{yl}–*Metal*–O_{yl} bonds (yl = O that belongs to uranyl) as in the case of both uranophanes or cuprosklodowskite, and O_{Si}–*Metal*–O_{Si} (Si = O atoms that are linked to Si) as in the case of sklodowskite. The additional linkage is provided through H-bonds that secure transfer of the charge from the interstitial cations to the sheets of polyhedra, the anionic part of the structure. Such a linkage is done by the action of transformer H_2O groups (O is 3-fold coordinated), linked to metal cation sites, through non-transformer H_2O groups (O is 4-fold coordinated), "free" H_2O not-bonded directly to any metal cation site, as well as by OH groups. These are localized, except for kasolite that does not contain any of OH, either at the free vertex (not linked to the *Me* site) of the Si-tetrahedron (cuprosklodowskite, uranophane-α, uranophane-β), or at the same vertex of the Si-tetrahedron, but linked to the interstitial *Me* site (sklodowskite, oursinite). In the case of sklodowskite, the position of the (OH) group was inferred mistakenly by [12]; however, in the case of oursinite, which is the derivative structure of sklodowskite, it has been localized properly by [17].

Sklodowskite (Figure 2c), $Mg[(UO_2)(SiO_3OH)]_2{\cdot}6H_2O$, and **cuprosklodowskite** (Figure 1d), $Cu[(UO_2)(SiO_3OH)]_2{\cdot}6H_2O$, have tightly related structures, differing in symmetry due to the presence of cations with distinct stereochemistry. The lowering from the *C*2/*m* (sklodowskite) (Figure 4b) to *P*–1 (cuprosklodowskite) is due to Jahn–Teller effect on Cu^{2+} in the octahedral crystal-field and a consequent change of coordination from O_h to C_{4v} (4 + 2). Therefore, the Cu in cuprosklodowskite is linked by the two longer bonds to O_{yl} atoms instead of the bonds towards O_{Si} atoms (Figure 4a).

Oursinite (Figure 2e), $(Co_{0.82}Mg_{0.18})_{\Sigma 1.00}[(UO_2)(SiO_3OH)]_2{\cdot}6H_2O$, is a derivative of the sklodowskite structure, where Co is substituting for Mg at the interlayer octahedrally coordinated *Me* site (Figure 4c). Interestingly, the current refinement provided practically the same Co:Mg ratio as reported in [17]. Moreover, few additional crystals were tested for the chemical composition on the electron microprobe; all preliminary results showed practically the same Co:Mg ratio for all checked crystals. It seems that Mg is essential there for the stabilization of the structure. Interestingly, the current structure refinement provided essentially the same peak in the difference Fourier map as [17]; this maximum is located ~1.6 Å from O_{yl} atom. A trial to refine this residual maximum as a partially occupied O site lowered *R* values considerably (drop down about 0.75%) and a goodness-of-fit (GOF) (about 0.5), however, yielded only a low population fraction and negative values of U_{eq}. Check for possible twinning, even considering oursinite as monoclinic with a halved unit-cell volume (twinned by the two-fold axis in 001*) did not lead to a better fit (many correlations among atom fractional coordinates and atomic displacement parameters) and or removal of this peak in the difference Fourier map.

Kasolite (Figure 2f), a Pb-dominant member of the uranophane group with the composition $Pb[(UO_2)(SiO_4)]{\cdot}H_2O$, is the only one known member of this class of minerals that do not contain protonated structural sheets. It is an effect of the incorporation of the large Pb^{2+} cation into the dense structure. Based on the structure refinement [19] it seems that the H_2O group in kasolite is a non-transformer, instead of the inverse transformer as suggested by [51].

Figure 2. (**a**) Prismatic crystals of uranophane-α in a vug of quartz-dominated gangue from the locality Swambo (Katanga province, Democratic Republic of Congo (DRC), Africa). Horizontal field of view (FOV) is 5.4 mm (photo P. Škácha). (**b**) Typical crystals of uranophane-β from the Rössing mine (Erongo, Namibia, Africa). Horizontal FOV is 5 mm (photo S. Wolfsried). (**c**) Crystals of sklodowskite on a quartz matrix from Kamoto-East open pit (Katanga province, DRC, Africa). Horizontal FOV is 5 mm (photo S. Wolfsried). (**d**) Cuprosklodowskite crystals a vug of Se-digenite rich matrix from the Musunoi mine (Katanga province, DRC, Africa). Horizontal FOV is 6 mm (photo S. Wolfsried). (**e**) Long needle-like oursinite crystals associated with becquerelite (orange) and rutherfordine (pale) from the Shinkolobwe mine (Katanga province, DRC, Africa). Horizontal FOV is 5 mm (photo S. Wolfsried). (**f**) Thick prismatic crystals of kasolite from the Musunoi mine (Katanga province, DRC, Africa). Horizontal FOV is 4 mm (photo S. Wolfsried). (**g**) Long prismatic crystals of boltwoodite from Goanicontes claim (Erongo, Namibia, Africa). Horizontal FOV is 14 mm (photo S. Wolfsried). (**h**) Fine thin prismatic crystals of swamboite-(Nd) in a vug with dipyramidal orange soddyite from the Swambo mine (Katanga province, DRC, Africa). Horizontal FOV is 3 mm (photo S. Wolfsried).

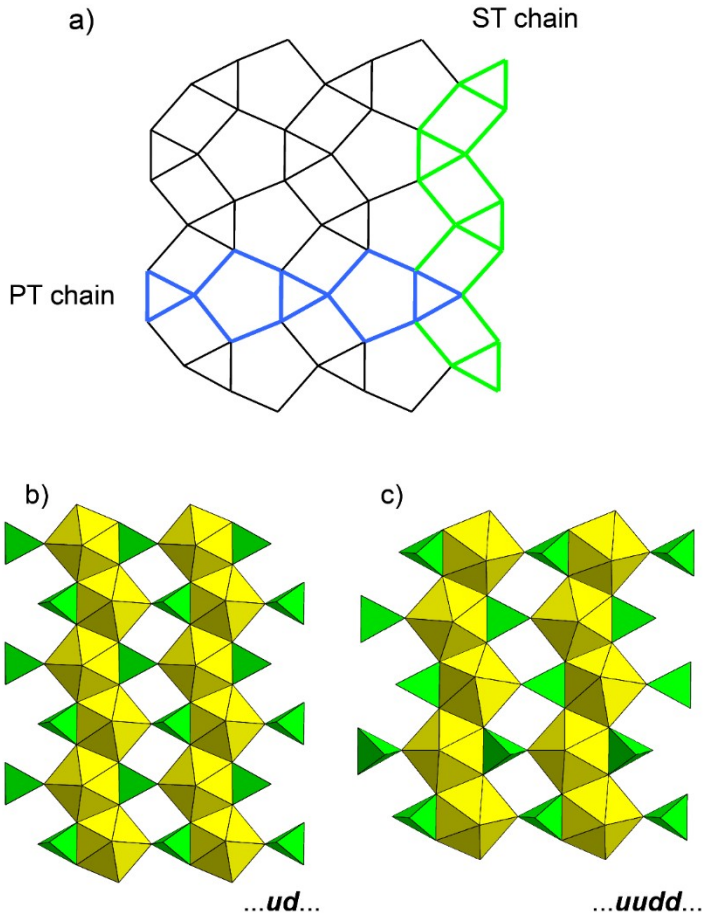

Figure 3. Uranophane uranyl-anion topology. (**a**) Its graphical representation with indicated pentagons-triangles (PT, blue) and squares-triangles (ST, green) chains. (**b**) Uranophane-α sheet projected onto (100). (**c**) uranophane-β sheet projected onto (010). UO_7 bipyramids are in yellow; SiO_4 tetrahedra are in green. The corresponding ST sequences are given.

Boltwoodite (Figure 2g), $K_2[(UO_2)(SiO_3OH)]_2 \cdot 3H_2O$, usually with a particular portion of K substituted by Na. The Na-rich variety is usually called natroboltwoodite (or earlier also sodiumboltwoodite). The reliable structure data were given by [35], documenting that boltwoodite is monoclinic (space-group $P2_1/m$), with the formula $(K_{0.56}Na_{0.42})[(UO_2)(SiO_3OH)](H_2O)_{1.5}$, obtained from the refinement of the structure and supported by the results of an electron microprobe analysis. The structure is based upon sheets with the uranophane anion-topology (***ud*** stereoisomer) and interlayer with four distinct atom sites that are partially occupied by one K (in seven-fold coordination), one Na (in six-fold coordination), and two O (of the H_2O groups) atoms. The structure and electron-microprobe study evidenced that there are not any H_3O^+ groups in the structure as assumed previously by [14]. Positions of H atoms in the structure of boltwoodite have not been determined so far.

Swamboite-(Nd) (Figure 2h), $Nd_{0.333}[(UO_2)(SiO_3OH)] \cdot 2.41H_2O$, is a particularly interesting member of the uranophane group in particular; its relation to this class of minerals has been established and elucidated recently [36]. Swamboite-(Nd) is one of only a few uranyl minerals with super-structural behavior. The effect of incorporation of highly charged Nd^{3+} cations between the $[(UO_2)(SiO_3OH)]^-$ uranophane-type of sheets and a low fraction of H_2O lead to both positional and occupational ordering of Nd^{3+} in the interlayer resulting in the (6, 3, 2) supercell of swamboite-(Nd).

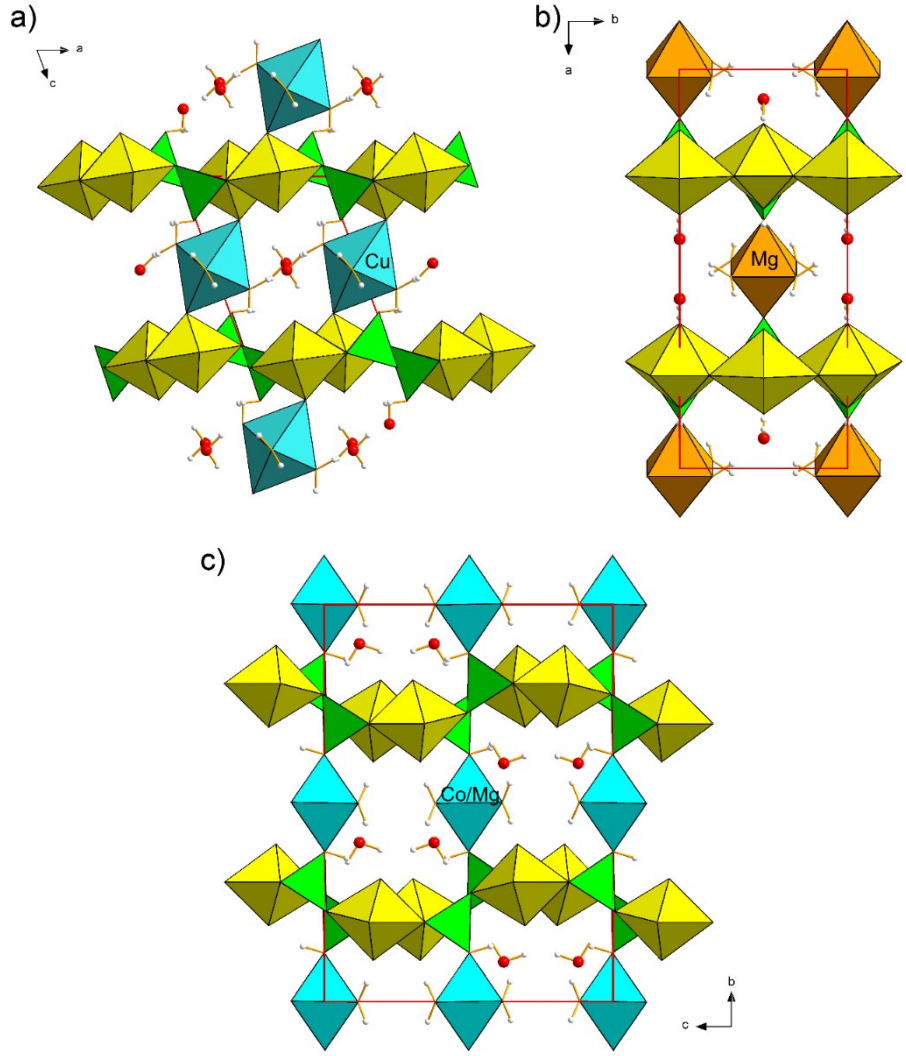

Figure 4. Crystal structures of minerals of the uranophane group (including H atoms). (**a**) Cuprosklodowskite. (**b**) Sklodowskite. (**c**) Oursinite. UO_7 bipyramids are in yellow; SiO_4 tetrahedra are in green, O atoms of the H_2O groups are in red, unit-cell edges outlined as red solid-lines.

3.2. Weeksite Group (2:5)

Weeksite group is characteristic for the structures with chains of SiO_4 tetrahedra. The mineral **weeksite** (Figure 5a), $K_2[(UO_2)_2(Si_5O_{13})]\cdot 4H_2O$, contains chains of edge-sharing UO_7 bipyramids that are linked by chains and sheets of vertex-sharing SiO_4 tetrahedra (Figure 6a). The sheets consist of 6-membered and 14-membered SiO_4 rings (Figure 6c) that are oriented perpendicular to the approximate plane formed by the equatorial ligands of the bipyramids. Therefore, these sheets both serve to link the chains of UO_7 into sheets and to link adjacent sheets together. Weeksite was considered to be an orthorhombic mineral in the past [52], but more recent investigations proved that crystals are usually twinned, and the real symmetry is monoclinic.

Haiweeite (Figure 5b), ideally $Ca[(UO_2)_2(SiO_3OH)_2(Si_3O_6)]\cdot 6H_2O$, is another naturally occurring uranyl silicate with 2:5 ratio. Noteworthy, its structure contains uranophane-type chains of edge-sharing UO_7 bipyramids with edge-sharing SiO_4 tetrahedra. Nevertheless, the linkages between these chains differ much from that of the uranophane group. In the structure of haiweeite, a complex network of SiO_4 tetrahedra links these chains of UO_7 bipyramids and SiO_4 tetrahedra, whereas, in the uranophane group, the chains are linked directly by sharing vertices. Adjacent sheets are then linked via Ca–O bonds and H-bonds [20] (Figure 6b).

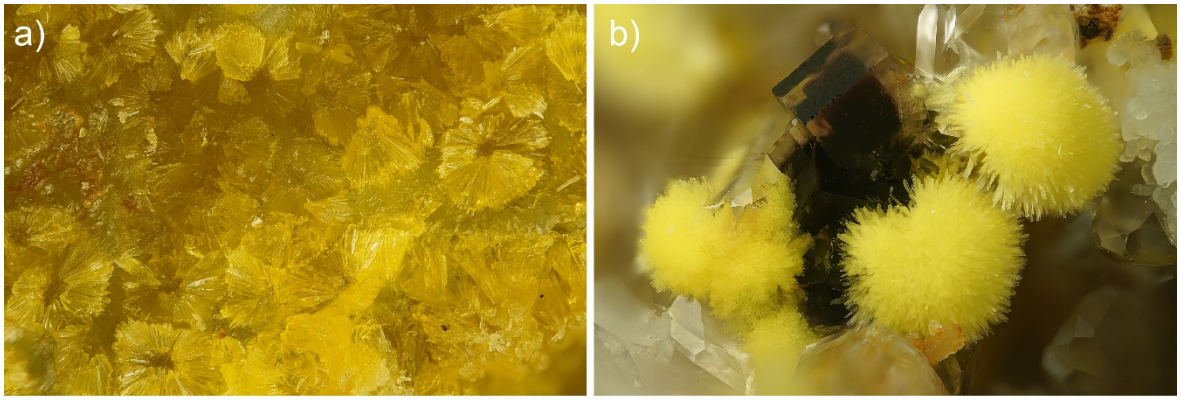

Figure 5. (**a**) Crystalline crust composed of weeksite long prismatic crystals on a specimen from the Anderson mine (Yavapai County, Utah, USA). Horizontal FOV is 3 mm (photo S. Wolfsried). (**b**) Long-prismatic fine crystals of haiweeite associated with quartz (colorless) and fluorite (dark) on a specimen from Teófilo Otoni (Mucuri valley, Minas Gerais, Brazil). Horizontal FOV is 4 mm (photo S. Wolfsried).

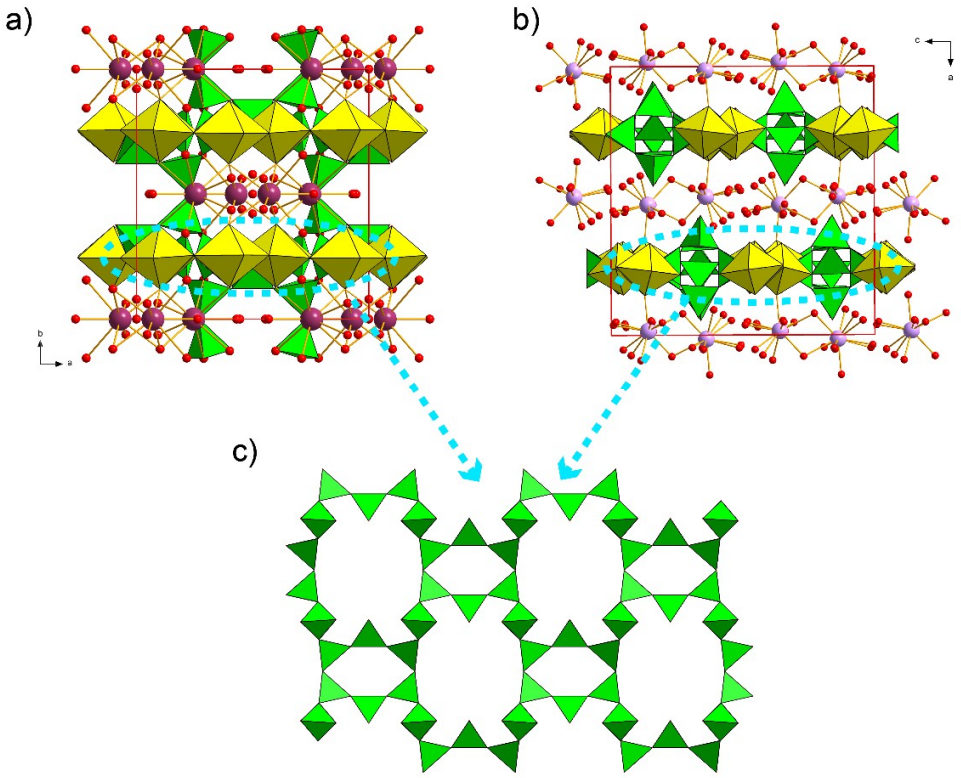

Figure 6. Crystal structures of weeksite-group minerals. (**a**) Weeksite viewed down [001]. UO_7 bipyramids are yellow, SiO_4 in green, K atom in violet, O atoms of the H_2O in red. (**b**) Haiweeite viewed down [001]. Color scheme same as previous, except of Ca atoms (lavender). (**c**) Silicate sheet resulting from sharing of six-membered rings of Si-tetrahedra, which is present in the structure of both minerals.

The structure of **coutihnoite**, $Th_xBa_{1-2x}(H_2O)_y[(UO_2)_2(Si_5O_{13})]\cdot 3H_2O$ (with $0 < x < 0.5$, $0 < y < (2 + x)$), remains unknown; however, the suggestion that it is related to the structure of weeksite has been made by [37], based on the stoichiometry and similarities in diffraction pattern.

3.3. Soddyite (2:1)

Soddyite (Figure 7a,b), $[(UO_2)_2(SiO_4)(H_2O)_2]$, the only mineral with the higher U:Si ratio than 1, has a topologically simple structure, where the chains of UO_7 bipyramids link directly through the sharing of SiO_4 edges [38].

Figure 7. (**a**) Yellow dipyramidal crystals of soddyite associated with pale rutherfordine on a specimen from the Musunoi mine (Katanga province, DRC, Africa). Horizontal FOV is 2 mm (photo S. Wolfsried). (**b**) Orange dipyramidal crystals of soddyite with minor swamboite-(Nd) (prismatic, needle-like) on a specimen from the Swambo mine (Katanga province, DRC, Africa). Horizontal FOV is 2 mm (photo S. Wolfsried).

4. Structural and Chemical Complexity of Uranyl Silicate Minerals

Complexity (information) measures for uranyl silicate minerals as calculated are given in Table 3; calculations were done taking into of account the H atoms. The median of $I_{G,total}$ values is 281 bits/cell (average is 1593 bits/cell); the distribution of the complexity values is highly asymmetric, showing a positive skewness (=3.161). Crystal structures of naturally occurring uranyl silicates can be characterized as simple (<100 bits/cell) to intermediate (100–500 bits/cell) regarding the information content. Nevertheless, there are few exceptions, reaching values of complexity making them complex, or very complex. Namely, it goes about uranophane–β (692 bits/cell), haiweeite (2314 bits/cell) and swamboite-(Nd). The last of those three minerals mentioned is worth more detailed comment.

Table 3. Uranyl silicate minerals and their complexity measures including H atoms.

Mineral	Spgr.	V (Å)	$D_{calc.}$	v	I_G	$I_{G,total}$	I_{Chem}
Soddyite	*Fddd*	1740	5.10	34	2.44	82.97	26.27
Boltwoodite	$P2_1/m$	321	4.14	32	3.75	120.00	27.11
Sklododowskite	$C2/m$	779	3.66	37	3.80	140.75	58.22
Cuprosklodowskite	$P\bar{1}$	384	3.89	37	4.24	156.75	60.39
Kasolite	$P2_1/c$	596	6.56	48	3.59	172.08	21.37
Oursinite	*Cmce*	2860	3.75	74	3.80	281.50	58.91
Uranophane-α	$P2_1$	736	3.83	68	5.09	345.95	56.47
Weeksite	$C2/m$	1809	3.80	82	4.70	385.32	67.57
Uranophane–β	$P2_1/c$	1428	3.98	136	5.09	691.90	56.47
Haiweeite	*Pbcn*	4667	3.08	408	5.67	2314.35	77.13
Swamboite-(Nd)	$P2_1/m$ #	404	3.73	26	3.39	88.21	25.39
	Super	14,391		1248	10.29	12,836.18	

Spgr.—space group; v—the number of vertices in the corresponding quotient graph; I_G—structural complexity contribution per atom (bits/atom); $I_{G,total}$—structural complexity of the whole structure (bits/cell); I_{Chem}—chemical information measures (bits/formula). #—average structure; Super—superstructure, space-group $P2_1/m(a1, b1, g1)00(-a1, b1, g1)00(a2, 0, g2)0s$.

The modulation in the structure of swamboite-(Nd) is a commensurate one; therefore, it can also be described by the super-cell. In Table 3, two values can, therefore, be found for swamboite-(Nd), one for average structure and a second for a superstructure. It is clear that the one for the average structure is a rough approximation only. The difference between those two numbers reflects the "amount of frustration". The calculation of complexity measures for modulated structures has not been established so far. However, it seems that for the commensurate case the super-cell approach should work. The number of 12,836.18 bits/cell makes swamboite-(Nd) extraordinarily complex, one of the most complex minerals in Nature, besides ewingite [53], $Mg_8Ca_8(UO_2)_{24}(CO_3)_{30}O_4(OH)_{12}(H_2O)_{138}$ (25,882.01 bits/cell; including H atoms—surrogated), ilmajokite, $(Na,Ca,Ba)_{10}Ti_5\ Si_{14}O_{22}(OH)_{44}{\cdot}nH_2O$ (7106.51 bits/cell; H atoms not considered) [54], and paulingite, $K_6Ca_{16}(Al_{38}Si_{130}O_{336})(H_2O)_{113}$ (6767.00 bits/cell) [47]. From the point of view of chemistry, uranyl silicates are relatively simple minerals (Table 3), none of which exceed 100 bits/formula. However, both weeksite and haiweeite, which also possess an increased structural complexity, belong to chemically less simple uranyl silicate minerals (Figure 8).

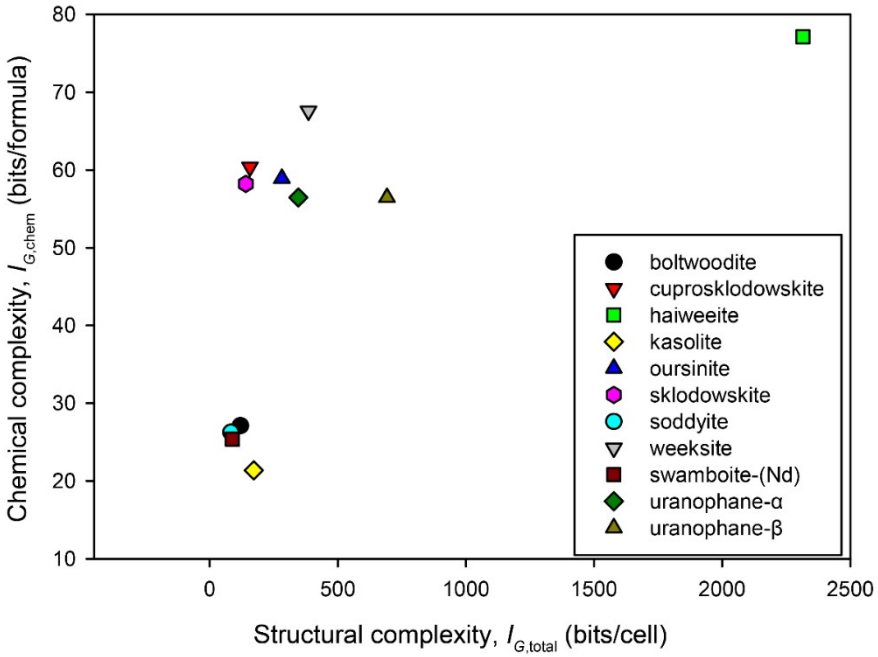

Figure 8. The relationship between the structural and chemical complexity of natural uranyl silicates (value of swamboite–(Nd) taken for the average structure; the value of the superstructure is taken as an outlier and is not shown).

5. Questionable, Poorly Defined or Unnamed Natural Uranyl Silicates

There are some questionable or poorly defined or even unnamed natural uranyl silicates, usually with a lack of detailed structural data. A short overview, which is given below, aims to provide a short review of available data for those phases that are either poorly defined minerals or related to the known minerals.

Calcioursilite, $Ca_4(UO_2)_4(Si_2O_5)_5(OH)_6{\cdot}15H_2O$, was described as a new mineral from the Oktyabr'skoye uranium deposit in Tajikistan by Chernikov in 1957 [40], but under the original name "ursilite". In 2018 [42] and references therein discredited "ursilite" as an old name and instead two mineral names were established: calcioursilite and magnioursilite. However, there is a particular controversy, because calcioursilite is considered as pentadecahydrate while magnioursilite as eikosahydrate, $Mg_4(UO_2)_4(Si_2O_5)_5(OH)_6{\cdot}20H_2O$. The difference in water content makes sense from the point of view of the crystal chemistry; nevertheless, it should be probably reflected by the nomenclature as well.

Metahaiweeite, $Ca[(UO_2)_2(SiO_3OH)_2(Si_3O_6)]\cdot nH_2O$ (where $n < 6$) has been mentioned in the original description [55] as a lower hydrate of haiweeite, being a part of partially dehydrated aggregates. There are neither any other relevant data on natural metahaiweeite nor any high-temperature X-ray studies available.

Orlite, $Pb_3(UO_2)_3(Si_2O_7)_2\cdot 6H_2O$, mentioned from an unknown locality in the former USSR by [56] differs in U:Si ratio from kasolite; however, the Pb:U ratio remains the same. If it goes about a self-standing mineral species or not, is hard to decide. Nevertheless, no material is available for the study and electron-microprobe studies of kasolite specimens from distinct localities did not show any significant deviations in U:Si ratio.

There are two different Ca-uranyl-silicate-titanate phases mentioned from the Dog mine, Ambrosia Lake, New Mexico, described under the codes UM1982-17-SiO:CaTiU and UM1982-19-SiO:TiU [57]. It goes about unique chemistry. Unfortunately, no additional or newer information is available.

Uranosilite, $UO_3\cdot 7SiO_2$, has been described by [43] from the Krunkelbach Valley Uranium deposit, Menzenschwand, the Black Forest Mountains, Baden-Württemberg, Germany. It is noteworthy that it has an extraordinary Si:U ratio among known phases, which does not resemble any known minerals or synthetic compounds.

A rather interesting unnamed mineral phase with the XRD pattern matching that of the synthetic $Ca_2(UO_2)_2(Si_2O_5)_3\cdot 10H_2O$ was reported from Jáchymov [58]. Nevertheless it has never been verified.

6. Laboratory Synthesis of Uranyl Silicates of the Uranophane-Group

Only few research papers report on the synthesis of analogs of naturally occurring uranyl silicate minerals. An interesting paper by Cesbron et al. [59] describes attempts to synthesize uranophane-β. They performed about fifty hydrothermal syntheses (at 150 °C) in steel autoclaves in order to obtain the uranyl silicates found at Nopal I uranium deposit in Mexiko, and to understand their conditions of formation. They reported that the products of the synthesis are weeksite, natroboltwoodite, its K- and (NH_4)-analogues and uranophane-α. Despite adopting various pH and temperatures, uranophane-β could not have been synthesized. The explanation has been given recently by [36]. Uranophane-α was obtained using aqueous solutions of uranyl acetate, calcium acetate, and sodium metasilicate as reagents. Interestingly, uranophane-α may crystallize from solutions of a broad range of Ca:Na ratios ranging from 0.5:2 to 4:2. At low concentrations of Ca, crystallization of boltwoodite and natroboltwoodite takes place, respectively. According to the experiment the acid pH (<5) is crucial to obtain good crystallinity of products; with the higher Si activity, crystallinity decreases.

An alternative way to obtain minerals of the uranophane group has been described in the paper by Vochten et al. [60] focused primarily onto a synthesis of boltwoodite. That was obtained by mixing a solution of uranyl nitrate and KCl in water at pH of 11.5 maintained by adding KOH. This solution was placed into a Teflon vessel in a Parr reaction bomb with a portion of synthetic hydrothermal quartz chunks. The reaction bomb was heated at 185 °C for seven days (under the pressure of ca. 1.3 MPa). After cooling to room temperature, the reaction mixture was found to be consisting of quartz fragments, a colloidal precipitate, and a crystalline phase of pale yellow needles and fine prismatic yellow crystals. Those were identified as boltwoodite. Time-dependent experiments showed that the yield of boltwoodite increases to a maximum after seven days, and then it decreased along with the formation of soddyite. The experiments that continued for 40 days or more provided crystals of soddyite only. The slow transformation of boltwoodite into soddyite was confirmed in separate experiments under the same conditions, later on, in which both natural and synthetic boltwoodite were suspended in distilled water. When the synthetic boltwoodite was placed into 2 M solution of $Ca(NO_3)_2$, $MgSO_4$, $Pb(NO_3)_2$ and NaCl enclosed in the Parr reaction autoclave for 24 h at 185 °C, uranophane-α, sklodowskite, kasolite and natroboltwoodite were obtained, based on identification by powder X-ray diffraction. Experiments running for more than fourty days yielded yellow prismatic crystals identified later as $Na_2(UO_2)_2(SiO_4)F_2$ [61].

7. Concluding Remarks

Uranyl silicates that occur in nature do not represent an extremely populated (about 16 members), but rather a widespread mineral group (uranophane-α has been reported from more than 900 localities all around the world). Among them, those of the uranophane topology are dominating, and furthermore, uranophane-α, the Ca^{2+}-dominant species, is by far the most common. This is probably a consequence of preferential precipitation of uranophane-type sheets from aqueous solutions due to their thermodynamic stability [32]. Nevertheless, the stability range of uranophanes (both –α and –β) is connected with more alkaline conditions than of soddyite, but approximately with the same activity of SiO_2 in the solution. Soddyite, similarly to a "simple" uranyl carbonate rutherfordine, $(UO_2)(CO_3)$, forms from the elementally-poor solutions of the relatively low pH. The formation of uranophanes is, therefore, connected with the later stages of alteration connected with the leaching of alkalis and alkaline earth elements from surrounding rocks. Unfortunately, there are not any available thermodynamic data for weeksite group of minerals; however, theoretical predictions based on the approach described in [62] show that both weeksite ($\Delta G_{0f,298}$ ~ −8825 kJ/mol) and haiweeite ($\Delta G_{0f,298}$ ~ −8993 kJ/mol) are both thermodynamically stable phases; the values of their Gibbs free energies of formation are even lower than of uranophane-α, −6193 kJ/mol [32]. Both minerals form under entirely distinct conditions than the uranophane group of minerals; the activity of Si should be rather high, which is reflected in a higher Si:U ratio. The typical association for weeksite and haiweeite is a silicate-dominating matrix.

In general, uranyl silicates have been observed as being formed under less oxidizing conditions compared to, e.g., uranyl phosphates and arsenates [6]. Although this can depend on local conditions at the particular locality, there are many documents that such a scenario is valid in general [63–66].

Supplementary Materials: The crystallographic information files (CIF) are available online at http://www.mdpi.com/2075-163X/8/12/551/s1.

Author Contributions: J.P. performed X-ray diffraction experiments, processed and interpreted diffraction data, ran the refinements, undertook calculations and wrote the paper.

Funding: This research received no external funding.

Acknowledgments: Simon Philippo (Musée national d'histoire naturelle, Luxembourg) and Jiří Sejkora (National Museum, Prague) are acknowledged for their help with obtaining samples for the study. Stephan Wolfsried is thanked for providing superb mineral photographs. This research was supported by the project no. LO1603 under the Ministry of Education, Youth and Sports National sustainability program I of the Czech Republic to J.P.

Conflicts of Interest: The author declares no conflict of interest.

References

1. Frondel, C. Systematic mineralogy of uranium and thorium. *US Geol. Surv. Bull.* **1958**, *1064*, 1–400. Available online: https://pubs.usgs.gov/bul/1064/report.pdf (accessed on 22 November 2018).
2. Finch, R.J.; Ewing, R.C. The corrosion of uraninite under oxidizing conditions. *J. Nucl. Mater.* **1992**, *190*, 133–156. [CrossRef]
3. Pearcy, E.C.; Prikryl, J.D.; Murphy, W.M.; Leslie, B.W. Alteration of uraninite from the Nopal-I deposit, Peña-Blanca district, Chihuahua, Mexico, compared to degradation of spent nuclear-fuel in the proposed United-States high-level nuclear waste repository at Yucca Mountain, Nevada. *Appl. Geochem.* **1994**, *9*, 713–732. [CrossRef]
4. Finch, R.J.; Murakami, T. Systematics and paragenesis of uranium minerals. In *Uranium: Mineralogy, Geochemistry and the Environment, Reviews in Mineralogy*; Burns, P.C., Ewing, R.C., Eds.; Mineralogical Society of America and Geochemical Society: Chantilly, VA, USA, 1999; Volume 38, pp. 91–179.
5. Krivovichev, S.V.; Plášil, J. Mineralogy and crystallography of uranium. In *Uranium: From Cradle to Grave*; Burns, P.C., Sigmon, G.E., Eds.; Mineralogical Association of Canada Short Courses: Quebec, QC, Canada, 2013; Volume 43, pp. 15–119.
6. Göb, S.; Guhring, J.E.; Bau, M.; Markl, G. Remobilization of U and REE and the formation of secondary minerals in oxidized U deposits. *Am. Mineral.* **2013**, *98*, 530–548. [CrossRef]

7. Wilson, C.N. Results from long-term dissolution tests using oxidized spent fuel. In *Scientific Basis for Nuclear Waste Management XIV*; Abrajano, T.A., Jr., Johnson, L.H., Eds.; Materials Research Society Symposia Proceedings: Boston, MA, USA, 1991; Volume 212, pp. 197–204.
8. Finn, P.A.; Hoh, J.C.; Wolf, S.F.; Slater, S.A.; Bates, J.K. The release of uranium, plutonium, cesium, strontium, technetium and iodine from spent fuel under unsaturated conditions. *Radiochim. Acta* **1996**, *74*, 65–71. [CrossRef]
9. Wronkiewicz, D.J.; Bates, J.K.; Wolf, S.F.; Bick, E.C. Ten-year results from unsaturated drip tests with UO_2 at 90 °C: Implications for the corrosion of spent nuclear fuel. *J. Nucl. Mater.* **1996**, *238*, 78–95. [CrossRef]
10. Maher, K.; Bargar, J.R.; Brown, G.E., Jr. Environmental speciation of actinides. *Inorg. Chem.* **2003**, *52*, 3510–3532. [CrossRef] [PubMed]
11. Rosenzweig, A.; Ryan, R.R. Refinement of the crystal structure of cuprosklodowskite, $Cu(UO_2)_2(SiO_3OH)_2(H_2O)_6$. *Am. Mineral.* **1975**, *60*, 448–453.
12. Ryan, R.R.; Rosenzweig, A. Sklodowskite, $MgO{\cdot}2UO_3{\cdot}2SiO_2{\cdot}7H_2O$. *Cryst. Struct. Commun.* **1977**, *6*, 611–615.
13. Rosenzweig, A.; Ryan, R.R. Kasolite, $Pb(UO_2)(SiO_4)(H_2O)$. *Cryst. Struct. Commun.* **1977**, *6*, 617–621.
14. Stohl, F.V.; Smith, D.K. The crystal chemistry of uranyl silicate minerals. *Am. Mineral.* **1981**, *66*, 610–625.
15. Viswanathan, K.; Harneit, O. Refined crystal structure of beta-uranophane $Ca(UO_2)_2(SiO_3OH)_2(H_2O)_5$. *Am. Mineral.* **1986**, *71*, 1489–1493.
16. Ginderow, D. Structure de l'uranophane alpha, $Ca(UO_2)_2(SiO_3OH)_2{\cdot}5H_2O$. *Acta Crystallogr.* **1988**, *44*, 421–424.
17. Kubatko, K.-A.; Burns, P.C. A novel arrangement of silicate tetrahedra in the uranyl silicate sheet of oursinite, $(Co_{0.8}Mg_{0.2})[(UO_2)(SiO_3OH)]_2(H_2O)_6$. *Am. Mineral.* **2006**, *91*, 333–336. [CrossRef]
18. Fejfarová, K.; Plášil, J.; Yang, H.; Čejka, J.; Dušek, M.; Downs, R.T.; Barkley, M.C.; Škoda, R. Revision of the crystal structure and chemical formula of weeksite, $K_2(UO_2)_2(Si_5O_{13}){\cdot}4H_2O$. *Am. Mineral.* **2012**, *97*, 750–754. [CrossRef]
19. Fejfarová, K.; Dušek, M.; Plášil, J.; Čejka, J.; Sejkora, J.; Škoda, R. Reinvestigation of the crystal structure of kasolite, $Pb[(UO_2)(SiO_4)](H_2O)$, an important alteration product of uraninite, UO_{2+x}. *J. Nucl. Mater.* **2013**, *434*, 461–467. [CrossRef]
20. Plášil, J.; Fejfarová, K.; Čejka, J.; Dušek, M.; Škoda, R.; Sejkora, J. Revision of the crystal structure and chemical formula of haiweeite, $Ca(UO_2)_2(Si_5O_{12})(OH)_2.6H_2O$. *Am. Mineral.* **2013**, *98*, 718–723. [CrossRef]
21. Čejka, J. Infrared spectroscopy and thermal analysis of the uranyl minerals. In *Uranium: Mineralogy, Geochemistry, and the Environment, Reviews in Mineralogy*; Burns, P.C., Finch, R.J., Eds.; Mineralogical Society of America: Washington, DC, USA, 1999; Volume 38, pp. 521–622.
22. Lu, G.; Haes, A.J.; Forbes, T.Z. Detection and identification of solids, surfaces, and solutions of uranium using vibrational spectroscopy. *Coord. Chem. Rev.* **2018**, *374*, 314–344. [CrossRef]
23. Morrison, G.; Smith, M.D.; Tran, T.T.; Halasyamani, P.S.; zur Loye, H.-C. Synthesis and structure of the new pentanary uranium(vi) silicate, $K_4CaUSi_4O_{14}$, a member of a structural family related to fresnoite. *CrystEngComm* **2015**, *17*, 4218–4224. [CrossRef]
24. Morrison, G.; Smith, M.D.; zur Loye, H.-C. Understanding the Formation of Salt-Inclusion Phases: An Enhanced Flux Growth Method for the Targeted Synthesis of Salt-Inclusion Cesium Halide Uranyl Silicates. *J. Am. Chem. Soc.* **2016**, *138*, 7121–7129. [CrossRef] [PubMed]
25. Morrison, G.; Tran, T.T.; Halasyamani, P.S.; zur Loye, H.-C. $K_8(K_5F)U_6Si_8O_{40}$: An Intergrowth Uranyl Silicate. *Inorg. Chem.* **2016**, *55*, 3215–3217. [CrossRef] [PubMed]
26. Chen, Y.H.; Liu, H.K.; Chang, W.J.; Tzou, D.L.; Lii, K.H. High-temperature, high-pressure hydrothermal synthesis, characterization, and structural relationships of mixed-alkali metals uranyl silicates. *J. Solid State Chem.* **2016**, *236*, 55–60. [CrossRef]
27. Morrison, G.; zur Loye, H.-C. Flux Growth of $[NaK_6F][(UO_2)_3(Si_2O_7)_2]$ and $[KK_6Cl][(UO_2)_3(Si_2O_7)_2]$: The Effect of Surface Area to Volume Ratios on Reaction Products. *Cryst. Growth Des.* **2016**, *16*, 1294–1299. [CrossRef]
28. Morrison, G.; Smith, M.D.; zur Loye, H.-C. Flux versus Hydrothermal Growth: Polymorphism of $A_2(UO_2)Si_2O_6$ (A = Rb, Cs). *Inorg. Chem.* **2017**, *56*, 1053–1056. [CrossRef] [PubMed]
29. Li, H.; Kegler, P.; Bosbach, D.; Alekseev, E.V. Hydrothermal Synthesis, Study, and Classification of Microporous Uranium Silicates and Germanates. *Inorg. Chem.* **2018**, *57*, 4745–4756. [CrossRef] [PubMed]

30. Gorman-Lewis, D.; Mazeina, L.; Fein, J.B.; Szymanovski, J.E.S.; Burns, P.C.; Navrotsky, A. Thermodynamic properties of soddyite from solubility and calorimetry measurements. *J. Chem. Thermodyn.* **2007**, *39*, 568–575. [CrossRef]
31. Shvareva, T.; Mazeina, L.; Gorman-Lewis, D.; Burns, P.C.; Szymanovski, J.E.S.; Fein, J.B.; Navrotsky, A. Thermodynamic characterization of boltwoodite and uranophane: Enthalpy of formation and aqueous solubility. *Geochim. Cosmochim. Acta* **2011**, *75*, 5269–5282. [CrossRef]
32. Shvareva, T.Y.; Fein, J.B.; Navrotsky, A. Thermodynamic properties of uranyl minerals: Constraints from calorimetry and solubility measurements. *Ind. Eng. Chem. Res.* **2012**, *51*, 607–613. [CrossRef]
33. Colmenero, F.; Bonales, L.J.; Cobos, J.; Timón, V. Structural, mechanical and vibrational study of uranyl silicate mineral soddyite by DFT calculations. *J. Solid State Chem.* **2017**, *253*, 249–257. [CrossRef]
34. Colmenero, F.; Fernández, A.-M.; Cobos, J.; Timón, V. Thermodynamic Properties of Uranyl-Containing Materials Based on Density Functional Theory. *J. Phys. Chem. C* **2018**, *122*, 5254–5267. [CrossRef]
35. Burns, P.C. The structure of boltwoodite and implications of solid solution toward sodium boltwoodite. *Can. Mineral.* **1998**, *36*, 1069–1075.
36. Plášil, J. Structural complexity of uranophane and uranophane-β: Implications for their formation and occurrence. *Eur. J. Mineral.* **2018**, *30*, 253–257. [CrossRef]
37. Plášil, J.; Petříček, V.; Locock, A.J.; Škoda, R.; Burns, P.C. The (3+3) commensurately modulated structure of the uranyl silicate mineral swamboite-(Nd), $Nd_{0.333}[(UO_2)(SiO_3OH)](H_2O)_{2.41}$. *Z. Kristallogr.* **2018**, *233*, 223–232. [CrossRef]
38. Atencio, D.; Carvalho, F.M.S.; Matioli, P.A. Coutinhoite, a new thorium uranyl silicate hydrate, from Urucum mine, Galileia, Minas Gerais, Brazil. *Am. Mineral.* **2014**, *89*, 721–724. [CrossRef]
39. Demartin, F.; Gramaccioli, C.M.; Pilati, T. The importance of accurate crystal-structure determination of uranium minerals. II. Soddyite $(UO_2)_2(SiO_4).2H_2O$. *Acta Cryst. C* **1992**, *48*, 1–4. [CrossRef]
40. Chernikov, A.A.; Krumetskaia, O.V.; Sidel'nikova, V.D. Ursilite—A new silicate of uranium. *Atom. Energ. Vop. Geol. Urana* **1957**, *6*, 61–65.
41. United Nations. Proceedings of the 2nd United Nations International Conference on the Peaceful Uses of Atomic Energy, Geneva, Switzerland, 1–13 September 1958; Volume 2, pp. 298–299.
42. Halenius, U.; Hatert, F.; Pasero, M.; Mills, S.J. IMA Commission on New Minerals, Nomenclature and Classification (CNMNC) Newsletter 43. *Mineral. Mag.* **2018**, *82*, 779–785. [CrossRef]
43. Walenta, K. Uranosilite, ein neues Mineral aus der Uranlagerstätte von Menzenschwand im südlichen Schwarzwald. *Neu. Jahrb. Mineral. Monatsh* **1983**, *6*, 259–269. (In Germany)
44. Rigaku Oxford Diffraction. *CrysAlisCCD, CrysAlisRED and CrysAlisPRO*; Oxford Diffraction Ltd.: Oxford, UK, 2017.
45. Sheldrick, G.M. SHELXT—Integrated space-group and crystal-structure determination. *Acta Cryst. A* **2015**, *71*, 3–8. [CrossRef] [PubMed]
46. Petříček, V.; Dušek, M.; Palatinus, L. Crystallographic computing system Jana 2006: General features. *Z. Kristallogr.* **2014**, *229*, 345–352.
47. Krivovichev, S.V. Topological complexity of crystal structures: Quantitative approach. *Acta Cryst. A* **2012**, *68*, 393–398. [CrossRef] [PubMed]
48. Krivovichev, S.V. Structural complexity of minerals: Information storage and processing in the mineral world. *Mineral. Mag.* **2013**, *77*, 275–326. [CrossRef]
49. Blatov, V.A.; Shevchenko, A.P.; Proserpio, D.M. Applied topological analysis of crystal structures with the program package ToposPro. *Cryst. Growth Des.* **2014**, *14*, 3576–3586. [CrossRef]
50. Siidra, O.; Zenko, D.S.; Krivovichev, S.V. Structural complexity of lead silicates: Crystal structure of $Pb_{21}[Si_7O_{22}]_2[Si_4O_{13}]$ and its comparison to hyttsjoite. *Am. Mineral.* **2014**, *99*, 817–823. [CrossRef]
51. Schindler, M.; Hawthorne, F.C. The stereochemistry and chemical composition of interstitial complexes in uranyl–oxysalt minerals. *Can. Mineral.* **2008**, *46*, 467–501. [CrossRef]
52. Jackson, J.M.; Burns, P.C. A re-evaluation of the structure of weeksite, a uranyl silicate framework mineral. *Can. Mineral* **2001**, *39*, 187–195. [CrossRef]
53. Olds, T.A.; Plášil, J.; Kampf, A.R.; Simonetti, A.; Sadergaski, L.R.; Chen, Y.S.; Burns, P.C. Ewingite: Earth's most complex mineral. *Geology* **2017**, *45*, 1007–1010. [CrossRef]

54. Zolotarev, A.; Krivovichev, S.; Zhitova, E.; Matteo, L.; Lyalina, L. The crystal structure and structural complexity of ilmajokite. In Proceedings of the XII Meeting of the International Mineralogical Associaiton, Book of Abstracts, Melbourne, Australia, 13–17 August 2018; p. 244.
55. McBurney, T.C.; Murdoch, J. Haiweeite, a new uranium mineral from California. *Am. Mineral.* **1959**, *44*, 839–843.
56. Fleischer, M. New mineral names. *Am. Mineral.* **1980**, *65*, 1065–1070.
57. Simova, F.G. Uranium-titanium silicates from the Ambrosia Lake (New Mexico, USA) and Mitterberg (Salzburg, Austria) deposits. *Bulg. Akad. Nauk. Doklady* **1982**, *35*, 203–206.
58. Ondruš, P.; Veselovský, F.; Skála, R.; Císařová, I.; Hloušek, J.; Frýda, J.; Vavřín, I.; Čejka, J.; Gabašová, A. New naturally occurring phases of secondary origin from Jáchymov (Joachimsthal). *J. Czech Geol. Soc.* **1997**, *42*, 77–108.
59. Cesbron, F.; Ildefonse, P.; Sichere, M.-C. New mineralogical data on uranophane and β-uranophane; synthesis of uranophane. *Mineral. Mag.* **1993**, *57*, 301–308. [CrossRef]
60. Vochten, R.; Blaton, N.; Peeters, O.; Van Springel, K.; Van Haverbeke, L. A new method of synthesis of boltwoodite and of formation of sodium boltwoodite, uranophane, sklodowskite and kasolite from boltwoodite. *Can. Mineral.* **1997**, *35*, 735–741.
61. Blaton, N.; Vochten, R.; Peeters, O.M.; Van Springel, K. The crystal structure of $Na_2(UO_2)_2SiO_4F_2$, a compound structurally related to soddyite, and formed during uranyl silicate synthesis in Teflon lined bombs. *N. Jahrb. Mineral. Monatsh.* **1999**, *6*, 253–264.
62. Chen, F.; Ewing, R.C.; Clark, S.B. The Gibbs free energies and enthalpies of formation of U^{6+} phases: An empirical method of prediction. *Am. Mineral.* **1999**, *84*, 650–664. [CrossRef]
63. Murakami, T.; Ohnuki, T.; Isobe, H.; Sato, T. Mobility of uranium during weathering. *Am. Mineral.* **1997**, *82*, 888–899. [CrossRef]
64. Ondruš, P.; Veselovský, F.; Gabašová, A.; Drábek, M.; Dobeš, P.; Malý, K.; Hloušek, J.; Sejkora, J. Ore-forming processes and mineral parageneses of the Jáchymov ore district. *J. Czech Geol. Soc.* **2003**, *48*, 157–192.
65. Plášil, J.; Sejkora, J.; Ondruš, P.; Veselovský, F.; Beran, P.; Goliáš, V. Supergene minerals in the Horní Slavkov uranium ore district, Czech Republic. *J. Czech Geol. Soc.* **2006**, *51*, 149–158. [CrossRef]
66. Plášil, J.; Sejkora, J.; Čejka, J.; Škoda, R.; Goliáš, V. Supergene mineralization of the Medvědín uranium deposit, Krkonoše Mountains, Czech Republic. *J. Geosci.* **2009**, *54*, 15–56. [CrossRef]